

## FWI in extended domain using time-warping

Guanghui Huang\*, Jaime Ramos-Martínez, Yang Yang and Nizar Chemingui, PGS

### Summary

The automation of model building using Full Waveform Inversion (FWI) depends on the lowest frequencies available in the data and an accurate initial model to avoid cycle-skipping. To overcome the cycle-skipping, a new class of FWI approaches extend the solution search in one or more dimensions. We present a new method that uses the time-warping function as the extension in the data space. This function dynamically transports the recorded data to the synthetic data and is imposed to represent the actual physical time. The resulting FWI objective function enables the solution of two parameters, velocity model and time-warping extension, in a single optimization problem, which is solved by the Alternate Direction Method (ADM). The mapping function is found by Dynamic Time Warping (DTW) with an augmented cost function provided by the time-warping extension. The novel FWI objective function, allows automatic transition from a pure time-shift problem to a conventional FWI. We apply the new FWI method to both synthetic and field data to demonstrate its effectiveness starting from inaccurate initial models. Results show that the new FWI approach is able to build high-resolution models from very simple initial velocity models.

### Introduction

FWI is a nonlinear optimization problem that matches modeled data to recorded field data (Tarantola, 1984). Typically, a least-squares objective function measures the data misfit. The non-convexity resulting from a least-squares objective function can cause FWI to converge to local minima. This problem, also known as cycle-skipping, is caused by lack of low-frequencies in the data and/or an inaccurate initial model.

In practice, starting FWI from the lowest useable frequencies and the smallest offsets may solve cycle-skipping. This requires intensive intervention, affecting the cost and turnaround of the project and reducing the opportunities for model building automation. Different strategies have been proposed to overcome the cycle-skipping problem. Wang et al. (2016) and Yao et al. (2019) introduced a workflow that generated a series of intermediate datasets by shifting the field data within half a cycle from the synthetic data. Then, they applied a conventional least-squares FWI for inverting the resulting intermediate datasets successively. Ma and Hale (2013) proposed to minimize travel time shifts estimated by dynamic image warping (DIW) for updating the background velocity in reflection FWI. Among this variety, the domain extension is a class of methods that add

extra degrees of freedom in the model space to overcome cycle-skipping. The inversion is then reformulated to enforce the non-physical model extension to a physical one. The extension can be introduced either in the model space, like the time-lag extended reflectivity model (Biondi and Almomin, 2013) or in the data domain such as source extension (Huang et al., 2017) and receiver extension (Metivier et al., 2020). Data domain extensions are preferable because they avoid increasing the computational cost, in contrast to those model extension-based approaches that require more modeling realizations.

We introduce a novel method that minimizes the data fitting between the synthetic and the warped field data by imposing a constraint on the time-warping extension. This constraint requires that the time-warping extension becomes the physical time as the updated model approaches the global solution. We formulate a new objective function to solve for two parameters (velocity model and time-warping extension) in a single non-linear optimization problem. We apply the ADM to solve the cost function. The inner problem for the time-warping extension can be solved using dynamic programming similarly to classic DTW (Sakoe and Chiba, 1978) but with the aforementioned constraint on the warping extension. This is in contrast to existing DTW algorithms (e.g., Hale, 2013). Additional preconditioning along the spatial axis is also applied to enhance lateral coherency. The outer problem consists of updating the velocity model by a local optimization method. Thus, the new extended domain FWI approach automatically switches from a tomography term responsible of overcoming the cycle-skipping, to a conventional least-squares FWI term for retrieving a high-resolution velocity model.

First, we introduce our new extended-domain FWI objective function then we discuss its convexity properties with respect to the time shifts. Finally, we demonstrate the effectiveness of the new FWI algorithm using synthetic and field datasets starting from inaccurate initial models.

### FWI objective function using time-warping extension

We start by introducing the time-warping extension  $T(t)$  as a function of time so that the synthetic  $u(t)$  and warped field data  $d(T(t))$  are matched regardless of the initial model, *i.e.*:

$$u(t) = d(T(t)), \quad (1)$$

where the time-warping extension  $T(t)$  is non-negative and satisfies the conditions  $T(0) = 0$  and  $T(t_{max}) = t_{max}$ . As the velocity gets close to the target one, the time warping extension  $T(t)$  approaches the actual physical time  $t$ , *i.e.*,

## FWI with time-warping extension

$T(t) = t$ , so that the warped data  $d(T(t))$  becomes the actual field data  $d(t)$ . Combining this constraint with the data matching equation 1, we formulate our new FWI objective function as

$$J[m, T] = \frac{1}{2} \|F[m] - d(T(t))\|_2^2 + \frac{\lambda}{2} \|t - T\|_2^2, \quad (2)$$

where  $m$  is the velocity model,  $u = F[m]$  is the synthetic data,  $\lambda$  is a positive trade-off parameter,  $T(t)$  is the time-warping extension that dynamically transports the field data  $d$  towards the synthetic data  $u$  and the difference  $\tau(t) = t - T(t)$  is defined as the shift field which captures the relative time shifts between the synthetic and field data.

We apply ADM to the optimization problem described in equation 2. First, the inner problem is solved by minimizing  $J[m, T]$  over  $T$  for the time-warping extension using dynamic programming (e.g., Sakoe and Chiba, 1978). The resulting augmented cost function is

$$T[m] = \operatorname{argmin}_T \frac{1}{2} \|F[m] - d(T(t))\|_2^2 + \frac{\lambda}{2} \|t - T\|_2^2, \quad (3)$$

Additional constraints on the time-warping function can be applied in both time and spatial axes to enhance the lateral coherence (e.g., Ma and Hale, 2013). The outer problem is the minimization of the reduced objective function:

$$J_{red}[m] = \frac{1}{2} \|F[m] - d(T[m])\|_2^2 + \frac{\lambda}{2} \|t - T[m]\|_2^2, \quad (4)$$

Figure 1 shows the behavior of the reduced objective function 4 with time-warping extension for large, medium and small values of  $\lambda$  comparing with a least-squares FWI. As  $\lambda$  decreases, the reduced objective function to a least-squares objective function to the quadratic objective function which is related to the time shift and is responsible for tomographic updates.

### SYNTHETIC EXAMPLE

We validated our algorithm using a modified version of the Marmousi model that simulates a marine setting (Figure 2a). The synthetic data were generated in a frequency bandwidth of 5 to 10 Hz. The data contained no frequencies below 3 Hz and the maximum offset was 5.5 km. The initial model (Figure 2b) consisted of a 1D velocity function that linearly increases with depth from the water bottom. This simple model produces faster refracted events (Figure 2f) than those corresponding to the true model as indicated by the yellow arrows (Figure 2e). For comparison, we apply the conventional L2-norm based FWI and the novel FWI with time-warping extension without the separation of reflections and refractions. The inverted model using a conventional FWI (Figure 2c) is trapped in a local minimum due to the

severe cycle-skipping. In contrast, the inverted model from our approach (Figure 2d) accurately resembles the true model. This is validated by comparing the sample synthetic shot gather computed from the inverted models using the conventional (Figure 2g) and the new approach (Figure 2h) with the input data. Notice the good match of reflections in Figures 2e and 2h indicated by dotted yellow ellipses.

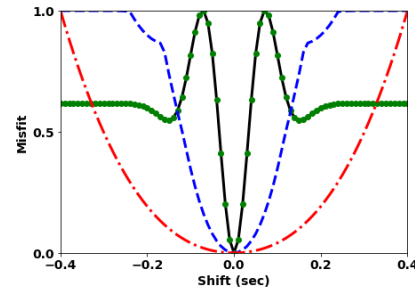


Figure 1: Normalized misfit function as a function of time shift for the Least-squares (solid black) and the reduced FWI objective functions with time-warping extension for large (dotted green), medium (dashed blue) and small (dash-dotted red) values of  $\lambda$ . The least-squares objective function completely coincides with the reduced FWI objective function for a large value of  $\lambda$ .

### FIELD DATA EXAMPLES

In this section, we describe the application of the new approach to two field datasets starting from very simple initial models. The first dataset corresponds to data acquired in offshore Malaysia, using the continuous wavefields method (Klüver et al., 2020). Multisensor streamers with a maximum inline offset of 8.1 km were deployed in a shallow water setting with depths between 125 m to 200 m. The initial model consisted of a linearly increasing velocity from the water bottom (Figure 3a). In Figure 3c, we show the comparison between the field and synthetic data from the initial model for the initial stage of the inversion with a maximum full power frequency of 6 Hz. As observed, at low frequencies and even at intermediate offsets, there is severe cycle-skipping in the refracted energy. In addition, the field data shows strong noise particularly at far offsets. We then perform the inversion up to a maximum frequency of 10 Hz and the result is depicted in Figure 3b. Results are validated by comparing the synthetic data computed from the inverted velocity model with the field data at different offsets (Figure 3d) for a maximum frequency 10 Hz. Waveform fit is nearly perfect, and it is difficult to determine the transition from the field to synthetic data in the displayed offset panels.

Finally, we apply our FWI with time-warping extension to data acquired in the Ceará Basin, offshore Fortaleza, Brazil. The acquisition comprises 14 multisensor streamers spaced 100 m apart, with a maximum inline offset of 8.1 km. The maximum frequency used in the inversion is 6 Hz. In the

## FWI with time-warping extension

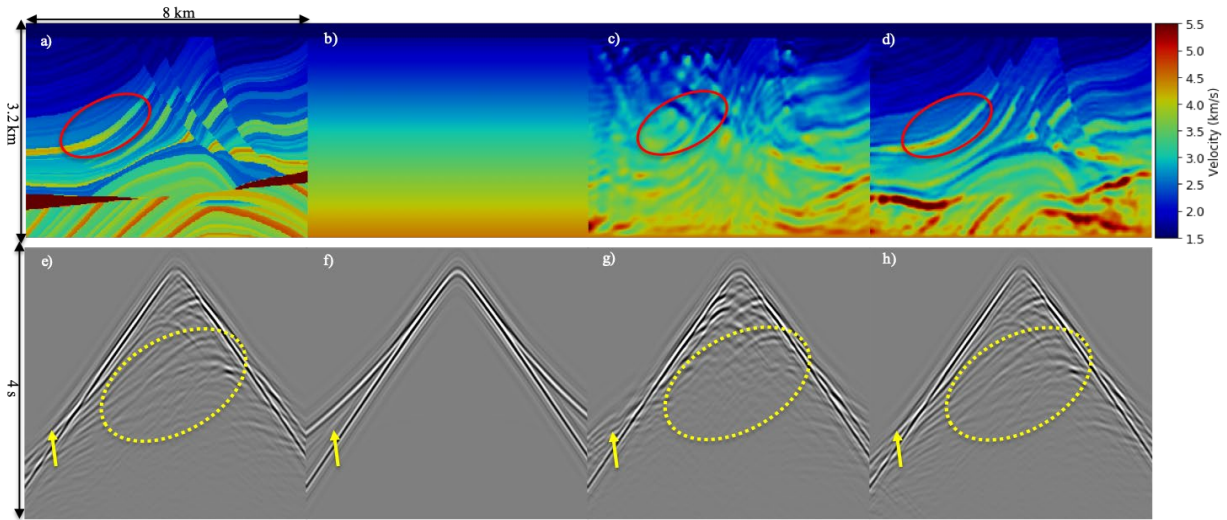


Figure 2: Synthetic example: (a) Marmousi model, (b) 1D initial model and FWI models using the (c) conventional and (d) time-warping extension approaches. (e) sample input shot gather, and the corresponding modeled data for the (f) initial, and the FWI models using the (g) conventional and the (h) extended domain approaches. For reference, yellow arrows at each panel indicate the arrival time of refracted energy at far offsets for the true model, which is only matched by the inverted model using the new approach.

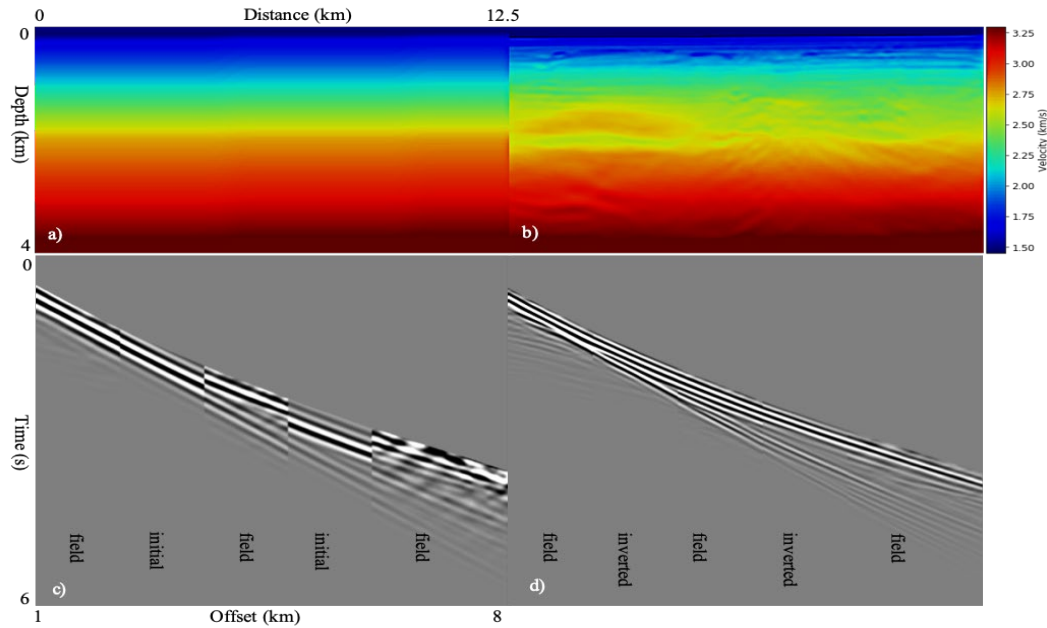


Figure 3. Malaysia field data example: (a) Initial and (b) inverted models using our approach; offset panels comparing field and synthetic data for (c) the initial model at 6 Hz and (d) the FWI model using our approach at 10 Hz.

shallow water area, according to well-log information, there is a heterogeneous carbonate layer with velocities up to 3500 m/s contrasting with those corresponding to the surrounding sediments (around 2500 m/s). We started the inversion from the model shown in Figure 4a, which corresponds to the

sediment velocities. Due to the high velocity contrast at shallow depths, the shot records contain mainly refracted energy with limited penetration. Cycle-skipping between the recorded refracted energy and the one simulated from the simple initial model is observed even at near offsets (Figure

## FWI with time-warping extension

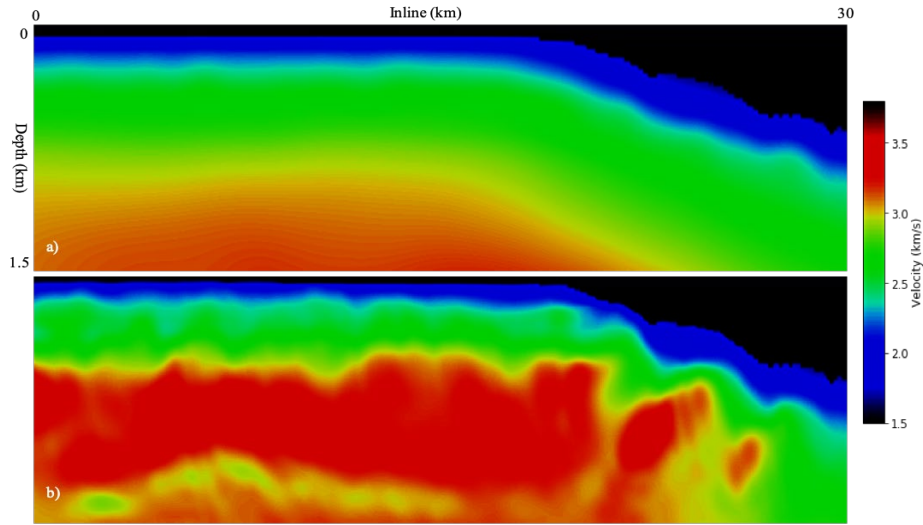


Figure 4: Brazil field data example: Inline corresponding to the (a) initial model and the (b) FWI model using our approach.

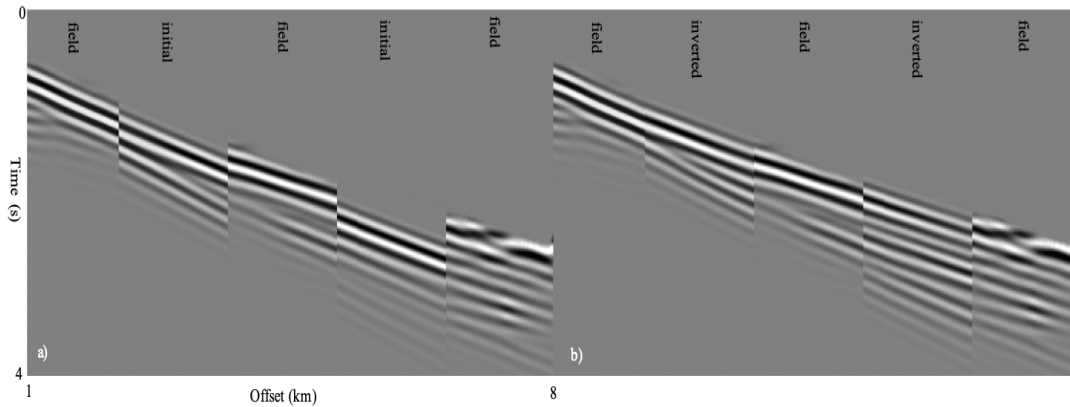


Figure 5: Brazil field data example: Comparisons of field and synthetic (offset panels) for data computed from the (a) initial and (b) FWI model using our approach.

5a). In Figure 4b, we show the FWI model obtained with our algorithm, which shows the spatial distribution of the carbonates with the range of velocities provided by the sonic logs. Figure 5b shows the validation of our solution at the early VMB stage. Note that the modeled data using our FWI model, reduces the cycle-skipping at all offset ranges.

### Conclusions

We have introduced a novel FWI objective function with time-warping extension to overcome cycle-skipping. The time-warping extension allows automatic transition from a tomography problem for overcoming cycle-skipping, to a conventional FWI problem for improving the resolution of

the velocity field. It is especially useful when data lacks low-frequencies, or the inversion starts from an inaccurate initial model. We successfully applied the new approach to field data to demonstrate that it is possible to retrieve high resolution velocity models starting from very simple initial models.

### Acknowledgments

We acknowledge the contributions of Sergey Frolov, Alejandro Valenciano and Odette Aragão during early stages of this study. We thank Stian Hegna and Tilman Klüver for assistance in the Malaysia dataset. We also thank Dan Whitmore, Tony Martin, Antonio Castiello and Ramzi Djebbi for numerous discussions.

## REFERENCES

- Biondi, B. and A. Almomin, 2013, Tomographic full-waveform inversion (TFWI) by combining FWI and wave-equation migration velocity analysis: *The Leading Edge*, **32**, 1074–1080, doi: <https://doi.org/10.1190/tle32091074.1>.
- Hale, D., 2013, Dynamic warping of seismic images: *Geophysics*, **78**, no. 2, S105–S115, doi: <https://doi.org/10.1190/geo2012-0327.1>.
- Huang, G., R. Nammour, and W. Symes, 2017, Full-waveform inversion via source-receiver extension: *Geophysics*, **82**, no. 3, R153–R171, doi: <https://doi.org/10.1190/geo2016-0301.1>.
- Ma, Y., and D. Hale, 2013, Wave-equation reflection travel-time inversion with dynamic warping and full-waveform inversion: *Geophysics*, **78**, no. 6, R223–R233, doi: <https://doi.org/10.1190/geo2013-0004.1>.
- Métivier, L., and R. Brossier, 2020, A receiver-extension approach to robust full waveform inversion: 90th Annual International Meeting, SEG, Expanded Abstracts, 641–645, doi: <https://doi.org/10.1190/segam2020-3425103.1>.
- Sakoe, H., and S. Chiba, 1978, Dynamic programming algorithm optimization for spoken word recognition: *IEEE Transactions on Acoustics, Speech, and Signal Processing*, **26**, 43–49, doi: <https://doi.org/10.1109/TASSP.1978.1163055>.
- Symes, W. W., 2008, Migration velocity analysis and waveform inversion: *Geophysical Prospecting*, **56**, 765–790, doi: <https://doi.org/10.1111/j.1365-2478.2008.00698.x>.
- Tarantola, A., 1984, Inversion of seismic reflection data in the acoustic approximation: *Geophysics*, **49**, 1259–1266, doi: <https://doi.org/10.1190/1.1441754>.
- Wang, M., Y. Xie, W. Q. Xu, F. C. Loh, K. Xin, B. L. Chuah, T. Manning, and S. Wolfarth, 2016, Dynamic-warping full-waveform inversion to overcome cycle skipping: 86th Annual International Meeting, SEG, Expanded Abstracts, 1273–1277, doi: <https://doi.org/10.1190/segam2016-13855951.1>.
- Yao, G., N. da Silva, M. Warner, D. Wu, and C. Yang, 2019, Tackling cycle skipping in full-waveform inversion with intermediate data: *Geophysics*, **84**, no. 3, R411–R427, doi: <https://doi.org/10.1190/geo2018-0096.1>.